Journal of Applied Physics

Extrinsic contributions to the dielectric and pyroelectric properties of $Pb_{0.99}[(Zr_{0.52}Ti_{0.48})_{0.98}Nb_{0.02}]O_3$ thin films on Si and Ni substrates

Cite as: J. Appl. Phys. **128**, 114102 (2020); https://doi.org/10.1063/5.0014405
Submitted: 19 May 2020 . Accepted: 26 August 2020 . Published Online: 16 September 2020

K. Coleman, S. Shetty, B Hanrahan, W. Zhu, and S. Trolier-McKinstry

Journal of Applied Physics ARTICLE scitation.org/journal/jap

Extrinsic contributions to the dielectric and pyroelectric properties of $Pb_{0.99}[(Zr_{0.52}Ti_{0.48})_{0.98}Nb_{0.02}]O_3$ thin films on Si and Ni substrates

Cite as: J. Appl. Phys. **128**, 114102 (2020); doi: 10.1063/5.0014405
Submitted: 19 May 2020 · Accepted: 26 August 2020 ·
Published Online: 16 September 2020

K. Coleman,[1,a)] S. Shetty,[1] B Hanrahan,[2] W. Zhu,[1] and S. Trolier-McKinstry[1]

AFFILIATIONS

[1]Materials Science and Engineering Department and Materials Research Institute, Pennsylvania State University, Millennium Science Complex, University Park, Pennsylvania 16802, USA
[2]U.S. Army Research Laboratory, Adelphi, Maryland 20783, USA

[a)]**Author to whom correspondence should be addressed:** kpc8@psu.edu

ABSTRACT

The character of extrinsic contributions to the dielectric and pyroelectric properties of $Pb_{0.99}[(Zr_{0.52}Ti_{0.48})_{0.98}Nb_{0.02}]O_3$ (PZT) films on Ni foil and Si wafers was explored using Rayleigh analysis, third harmonic phase angle, and Preisach analysis from 15 K to 296 K. The temperature dependence of the domain structure, domain wall mobility, and domain switching influenced the intrinsic, extrinsic, and secondary contributions to the pyroelectric coefficients. This, in turn, produced markedly different room temperature pyroelectric coefficients of $\sim 250\,\mu C/m^2\,K$ and $\sim 100\,\mu C/m^2\,K$, respectively, for films on Ni and Si. At room temperature, the dielectric irreversible Rayleigh parameter α_{ray} was 15.5 ± 0.1 and 28.4 ± 1.6 cm/kV for PZT on Si and Ni, respectively. The higher α_{ray} value for the Ni sample suggests more domain wall motion at room temperature, which was attributed to the lower stiffness on the Ni foil compared to the $\sim 500\,\mu m$ thick Si substrate. Below 200 K, α_{ray} for the PZT Si sample exceeds that of the Ni/PZT sample. This is believed to arise from differences in the energy landscape of pinning centers for the domain wall motion. It is proposed that the residual stresses not only set the preferred domain structures but also the barrier heights for domain wall motion and domain switching.

INTRODUCTION

Pyroelectric thin films are used in infrared imagers,[1–4] thermal energy harvesters,[5–7] and detectors of thermal infrared radiation.[2,8–12] The performance of these devices depends on the pyroelectric coefficient, π, of the film, which is determined by the change in polarization with temperature.[12] At the zero applied field (which is the condition for this paper), the change in polarization (or dielectric displacement, D) with temperature (T) depends on several factors as follows: [13,14]

$$\pi_{total} = \left(\frac{\partial D}{\partial T}\right)_x + \left(\frac{\partial D}{\partial \sigma}\right)_T \left(\frac{\partial \sigma}{\partial x}\right)_t \left(\frac{\partial x}{\partial T}\right)_\sigma + P_s\left(\frac{\partial \varphi_C}{\partial T}\right). \quad (1)$$

The primary pyroelectric response is due to the change in the magnitude of the spontaneous polarization (P_s) with temperature. There is also a secondary term due to a stress (σ) induced response due to the piezoelectric response of the film, which induces a polarization due to the change in dimensions (x = strain) associated with a temperature change.[7,13,15] Finally, there also can be an extrinsic contribution from the motion of domain walls or phase boundaries.[16] In the case where heating is not uniform, an additional term is also possible,[14] but this is typically negligible for thin films clamped to substrates with good thermal conductivity (such as Si and metallic substrates),[13] and so it is not included in Eq. (1). The combination of the secondary and extrinsic contributions can account for up to a third of the pyroelectric coefficient[17] with tuning of strain in the film. Studies show that changing the epitaxial strain and the thermal expansion mismatch between the film and substrate can increase the pyroelectric coefficient significantly.[7,17–19]

It is important to recognize, however, that thermal stresses will also modulate other contributions to the net pyroelectric effect. In particular, the thermal expansion mismatch stress between the film and the substrate influences the percentage of out-of-plane "c" and in-plane "a" domains in {001} oriented perovskite films with a significant tetragonal phase fraction.[20,21] This changes the primary pyroelectric coefficient. Additionally, changes in temperature and stress also influence the domain populations and types of domain walls present in the films, and hence, the extrinsic contributions to pyroelectricity.[7,17,22,23] Finally, local stresses in the film may pin certain types of domain walls[24] and determine the domain wall density[22] and domain structure.[17]

In PZT films, the extrinsic contribution to the pyroelectric coefficient is hard to predict due to the complex domain structure and various degrees of clamping. For example, a substrate's stiffness and thickness influence the degree of in-plane clamping experienced by the film[25,26] and thereby alter the extrinsic contributions to properties. Changes in the film's stress state can significantly alter the amount of domain wall motion; this has been demonstrated by the reduction of stress through releasing the films from the underlying substrate,[27,28] as well as by varying epitaxial strains.[17] However, to date, the relationship between stresses and domain wall pinning sites is not fully understood. This complicates the prediction of the functional pyroelectric, dielectric, and piezoelectric responses of ferroelectric thin films and reduces the accuracy of calculations on the high field response of sensors and actuators.

For example, stresses may affect the extent of domain wall motion at low fields and domain nucleation and growth at higher fields. Therefore, the influence of stresses should be explored using both low and high field methods. At lower fields, the dielectric non-linearities of many ferroelectrics can be described through the Rayleigh law[29,30] as

$$\varepsilon_r = \varepsilon_{init} + \alpha_{Ray} E_{ac}, \tag{2}$$

where $\varepsilon_{\text{init}}$ captures the response due to reversible domain wall motion and intrinsic contributions and α_{Ray} quantifies the irreversible domain wall motion (α_{Ray}) to the permittivity. Analysis of the Rayleigh response for films on various substrates[23,25] suggests that films with flexible substrates exhibit higher domain wall contributions to the properties than more fully clamped films on rigid substrates. Because the domain wall motion is thermally activated, temperature dependent Rayleigh measurements can provide one means of quantifying the depth of the potential wells pinning domain walls, since at low temperatures, mobile interfaces can be frozen out of the response.[31]

To confirm Rayleigh behavior at lower temperatures, the phase angles (δ_i) of the higher harmonics of the dielectric response can be used to determine the Rayleigh regime.[31,32] In particular, δ_3 should be at −90° (note a change in sign convention between Refs. 33 and 34 and Ref. 32). It has been shown that the phase angle may require a threshold field to reach the Rayleigh regime at some temperatures, which can give insight into the energy barrier ranges for the domain wall motion.

Additionally, Preisach distributions [or more generally first order reversal curve (FORC) distributions][35–37] describe the switching distributions over a much wider range of fields than is described by Rayleigh behavior.[37] These models describe switching in terms of a distribution of hysterons, where each hysteron has a characteristic positive switching field (E_f) and negative switching field (E_b).[37] It is assumed that E_f is greater than E_b. While this model does not illuminate the detailed mechanisms for switching, it does allow the temperature dependence of the switching distributions to be described. This is useful as the local coercive fields depend on the pinning of domains through imprint[38,39] and the variation in stresses[40,41] and clamping[41,42] of the films. Since the FORC distribution covers a higher field range, it probes a broader distribution of pinning centers, which may lead to different ideal poling conditions of films under different stress states. Determining these differences in energy barrier height for low field and high field conditions is necessary to fully quantify and exploit the extrinsic response of the film to optimize various properties.

In this work, the link between extrinsic contributions and the dielectric and pyroelectric properties based on stresses in 0.6 μm thick $Pb_{0.99}\square_{0.01}[(Zr_{0.52}Ti_{0.48})_{0.98}Nb_{0.02}]O_3$ (PZT) (note $\square$ represents lead vacancies) films on Ni and Si substrates were explored. Nb doped PZT was used since it has good piezoelectric and pyroelectric coefficients, a low leakage current, and is used in many commercial applications.[43–45] Rayleigh and Preisach analysis as well as δ_3 values were used to compare the domain wall motion at low fields and switching behavior at high fields from 10 K up to room temperature (296 K). From these results, working models of the potential energy landscapes and domain structure were developed to convey the differences in extrinsic contributions from one PZT thin film to another, based on residual stresses.

EXPERIMENTAL PROCEDURE

The PZT films used in this study were grown through chemical solution deposition (CSD) using a 2-methoxyethanol based solution[23,25,46] to a thickness of 0.6 μm on double-sided polished 500 μm Si ⟨001⟩ Nova Electronic Materials wafers with a 1 μm thick thermal oxide and 50 μm 99.98% pure Sigma Aldrich Ni foils that had a HfO_2 buffer layer to prevent diffusion along with oxidation.[25] A bottom electrode of lanthanum nickelate was used and a Pt top electrode. These films on both substrates had a morphotropic phase boundary composition with a preferred {001} orientation, and dense columnar grains, without the presences of any secondary phase. These films were used in a prior study,[23] and x-ray diffraction patterns and SEM images of these films can be found elsewhere.[23]

The pyroelectric coefficient of PZT on Ni and Si were measured by heating the substrates using a cartridge heater powered by a 50% duty cycle square wave while monitoring the temperature and sample current. Equation (3) relates the pyroelectric coefficient, π, to heating/cooling and sample properties,

$$\pi = \frac{I_\pi}{A\left(\frac{dT}{dt}\right)}, \tag{3}$$

where A is the current collection area, I_Π is the pyroelectric current, T is temperature, and t is time.

For the temperature measurement, a co-located, surrogate thin film platinum resistive thermal device (RTD) was used to estimate the pyroelectric thin film temperature. The thermal properties of the Ni and Si substrates were modeled to ensure the accuracy of the surrogate RTD chip.[18] Additional electrical characterization of the films was performed using a Lakeshore Cryotronics 8400 series temperature-controlled probe station from 10 K to 296 K. Samples were adhered to the stage using a thin layer of GE varnish to ensure good thermal contact. A Cernox thin film RTD cryogenic temperature sensor on a glass substrate was adhered on the stage using a thin layer of GE varnish near the samples to monitor the temperature. Measurements as a function of temperature were made on heating from 10 K.

First, polarization–electric field (P–E) hysteresis loops were measured using a custom-built electric field loop system using a AC voltage amplifier (790 series power amplifier Piezotronics Inc.) described elsewhere.[38,47] One set of loops was measured up to 400 kV/cm at 100 Hz, and the coercive field (E_c) and remanent polarization (P_r) were recorded. Since E_c drastically increases with decreasing temperature, polarization hysteresis loops were repeated at $4 \times E_c$ to obtain fully saturated loops.

Low field measurements of permittivity of PZT on Ni and Si were acquired using a Hewlett Packard LCR meter at 1 kHz and 30 mV AC signal.[34] The first, second, and third harmonics of the permittivity and their respective phase angles at 1 kHz were determined using a lock-in amplifier as an AC voltage source, which was swept up to half the coercive field at each temperature.[34] Rayleigh measurements of the permittivity were taken at 1 kHz using the LCR meter and AC signals up to 25 kV/cm. The Rayleigh parameters were determined by a linear best fit in the Rayleigh regime.[28]

To probe the dielectric response at higher fields, First Order Reversal Curves (FORCs) were measured using 40 loops that increased linearly in the field up to four times the coercive field, as described elsewhere.[38,47] The field range probed was from $-4E_c$ to $+4E_c$ at each temperature. The Preisach distribution was determined from these loops, as described elsewhere.[38,47]

RESULTS AND DISCUSSION

At room temperature, the pyroelectric coefficients of PZT films on Ni and Si substrates were found to be −251 and −106 μC/(m^2 K) respectively, with ±25% standard deviation. The higher value for the film on Ni is a function of the fact that this PZT film is under compressive stress and so has a higher remanent polarization.[19,20,23] The Curie temperatures, T_c, were measured to be ~320 °C for both films, see the supplementary material for more details. This suggests domain structure may alleviate some of the residual stresses, which is plausible given the complex domain states.[29,48]

There are several important points to note from the temperature dependence of the P–E hysteresis loops of PZT on Ni [Fig. 1(a)] and PZT on Si [Fig. 1(b)]. At $4E_c$, the P–E loops of PZT on Si above 150 K are not well saturated. For temperatures above 150 K, saturated loops of PZT on Si at higher fields were used for the P_r and E_c values in Figs. 1(c) and 1(d), respectively. As expected, both films showed a decrease in the P_r and E_c with an increase in temperature as shown in Figs. 1(c) and 1(d), respectively. E_c at 15 K was −257 kV/cm and 221 kV/cm for PZT on Ni, and −117 kV/cm and 104 kV/cm for PZT on Si, and at room temperature dropped to 43 kV/cm for PZT on Ni and 36 kV/cm for PZT on Si. Over the temperature range, E_c for PZT on Ni was roughly twice that of PZT on Si, as indicated by the dashed line.

At 15 K, P_r for PZT on Ni and Si was $47.5 \pm 1.4\,\mu$C/cm^2 and $19 \pm 2\,\mu$C/cm^2, respectively. From phenomenology, it is estimated that "c" domains for this composition at 15 K would have a spontaneous polarization, P_s, of ~61 μC/cm^2 and "a" domains would have no contribution to the out-of-plane polarization.[49] Assuming, as a first approximation, that these films have only "a" or "c" domains and that ferroelastic domain switching is absent at 10 K; since P_r will scale with P_s, the percentage of "c" domains can be estimated. At 15 K, PZT on Ni has ~80 vol. % of "c" domains at 15 K, and PZT on Si has ~30 vol. % of "c" domains. This is lower than room temperature reports for percentage of "c" domains of PZT on Si.[23,50] At room temperature, P_r is 26 μC/cm^2 (at $4 \times E_c$) for PZT film on Ni suggesting only ~50 vol. % of "c" domains.[23,49,50] However, in higher maximum electric fields (900 kV/cm), P_r further increases to 34.5 μC/, which would suggest ~65% "c" domains, which is lower than previous reports.[23] See the supplementary material for more details.

The difference in the volume fraction of "c" domains at 15 K and room temperature can be attributed to extrinsic contributions, changes in the domain structure due to domain reorientation with change in stress with temperature, or a combination of these. The stress changes in the film due to thermal expansion mismatch stress (σ_t) is defined by[23,51,52]

$$\sigma_t = \frac{\int_{T_c}^{T_{max}} (CTE_f - CTE_s)dT}{\left\{\frac{1-\nu_f}{Y_f} + \left(\frac{1-\nu_s}{Y_s}\right)\left(4\frac{t_f}{t_s}\right)\right\}}, \quad (4)$$

where CTE is the coefficient of thermal expansion, ν is the Poisson's ratio, Y is the Young's modulus, and t is the thickness for the film (f) and substrate (s).

For the temperature range used here (15 K–296 K), the CTE for Ni varies from 0.02 to 13.3 ppm/K[53,54] and Si from −0.5 to 2.6 ppm/K.[55,56] The CTE for PZT below 273 K has not been reported, but in the ferroelectric regime, CTE has been reported to be roughly 2 ppm/K.[20,57,58] The volumetric thermal expansion coefficient was estimated from the results in Refs. 59–61 and below 60 K, it is assumed that the CTE for PZT decreases linearly to 0 ppm/K as 0 K is approached for the calculation. Therefore, approximately −200 MPa and −5 MPa more stress is added to PZT on Ni and Si, respectively, when it is cooled from room temperature down to 15 K. The small change in stress for the sample on Si produces little ferroelastic switching, such that the volume fraction of "c" domains is approximately constant at cryogenic temperatures. The P_r of PZT films on Ni is expected to increase by ~2.5 μC/cm^2 under −200 MPa,[23] which suggests an increase in "c" domains as the temperature is reduced,[49] but additional contributions must be considered since there are limitations to these phenomenological assumptions.[48]

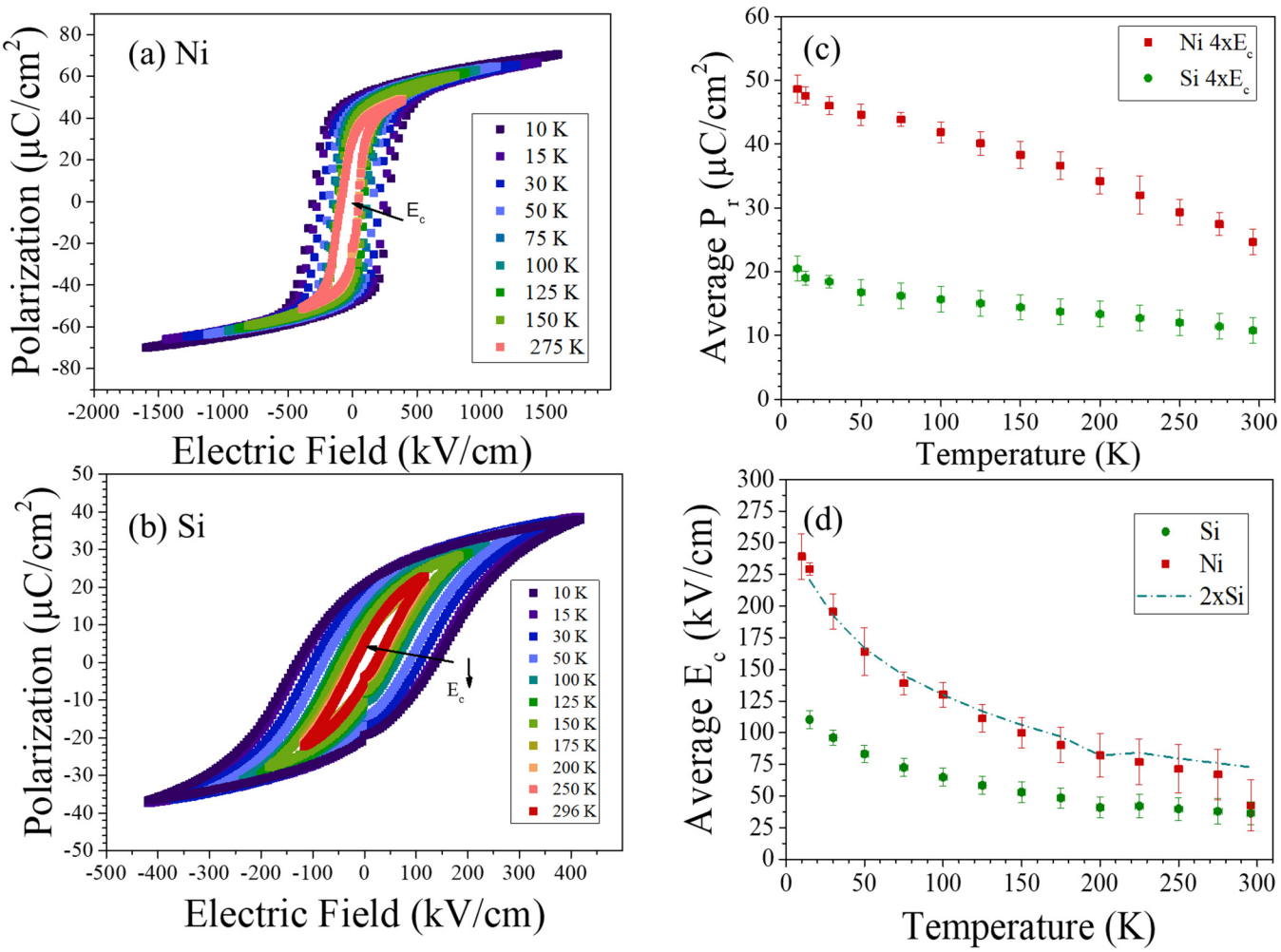

FIG. 1. *P–E* hysteresis loops for PZT on Ni (a) and Si (b). The remanent polarization (c) and coercive field (d) as a function of temperature for PZT on Ni (red squares) and on Si (green circles). E_c for PZT on Ni was roughly twice that of PZT on Si for all temperatures measured.

Rayleigh behavior and higher harmonics of the dielectric constant were investigated down to 10 K to determine the extent of domain wall motion at lower temperatures. At the onset of the Rayleigh regime, the phase angle of the third harmonic switches from −180° to −90° as domain walls begin to contribute to the permittivity[32] (note that the sign of the phase angle has been changed to be consistent with recent reports[33]). The first, second, and third harmonics are reported in the supplementary material. For perfect Rayleigh behavior in an unpoled sample, only the odd harmonics should be present.[62] However, small values for the second harmonic were seen and attributed to slight poling of the samples, which is consistent with previous studies on PZT films.[62]

Figure 2 shows that the third harmonic phase angle, δ_3, for PZT on Ni and Si shifts from −180° to −90° on increasing magnitude of the electric field. Consistent with previous reports,[32] there is a threshold field required to reach −90°, suggesting that the entire energy landscape distribution for domain wall motion is greater than 0 eV. As the temperature decreases, the AC field required to reach the Rayleigh-like regime rises. The field where the third harmonic phase angle first reaches −90 ± 5° is denoted as $E_{\delta 3}$. It is notable that there is a larger deviation from the 90° phase angle for films on Si, relative to films on Ni. The results were reproducible; the origin of this behavior is not known but may indicate an additional conduction mechanism. This may cause additional errors with determining $E_{\delta 3}$. PZT on Ni shows a greater temperature dependence, where at 296 K, $E_{\delta 3}$ is 5.8 ± 0.8 kV/cm and at 75 K, $E_{\delta 3}$ is 19 ± 0.8 kV/cm. For PZT on Si, $E_{\delta 3}$ is ∼5.8 ± 0.8 kV/cm at room temperature and increased to ∼0.2 ± 0.8 kV/cm at 75 K.

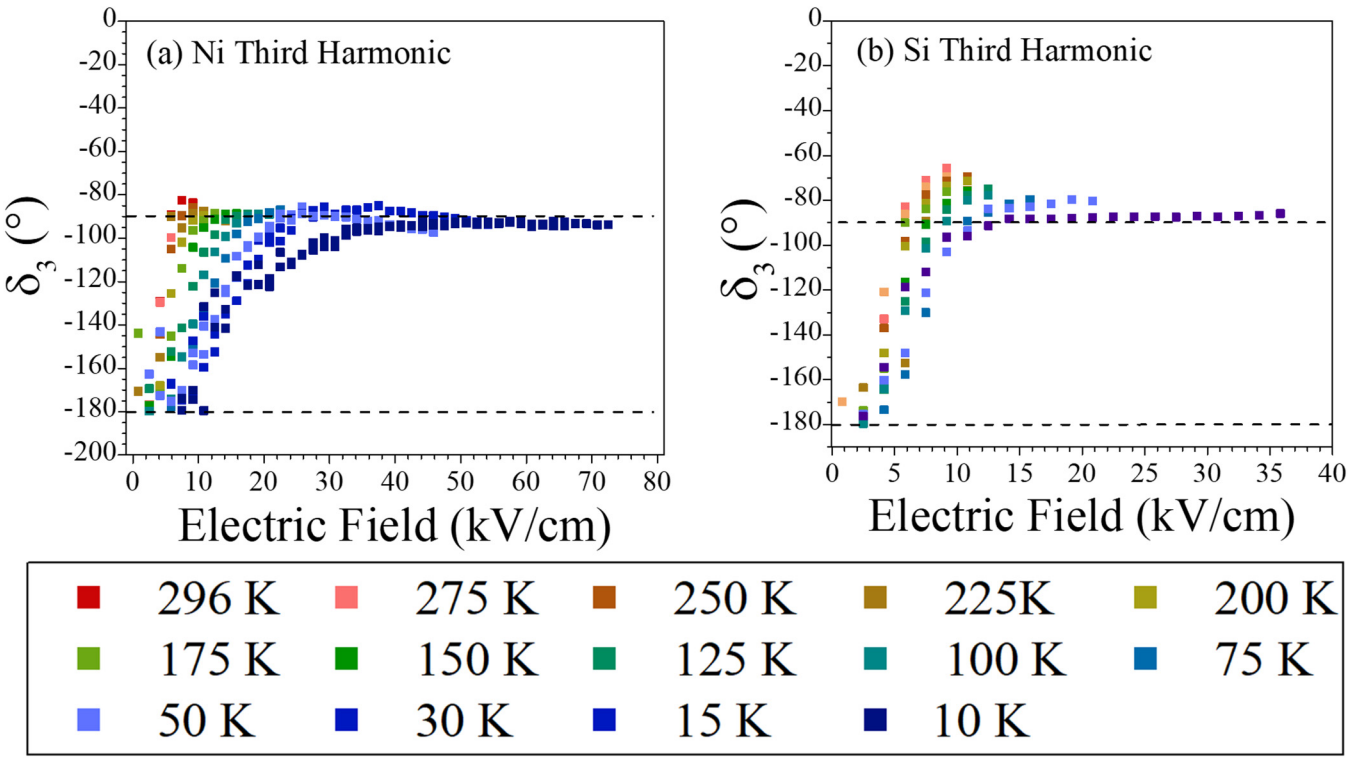

FIG. 2. Third harmonic phase angle, δ_3, for PZT on Ni (a) and on Si (b) from room temperature down to 10 K. The field (E_{δ_3}), where the phase angle reached −90° ± 5 is used as a proxy for defining when Rayleigh-like behavior was present. As the temperature decreases, $E_{\delta 3}$ increases. This temperature dependence is shown to be greater for PZT on Ni as seen by the larger electric field required to reach a −90° phase angle.

Figure 3 plots $E_{\delta 3}$ vs E_c. For all temperatures investigated, the Rayleigh-like behavior begins at a consistent percentage of E_c. For PZT on Ni. $E_{\delta 3}$ ranges from 7 to 15% of E_c, for both films at the various temperatures. This slight differences at each temperature may suggest that there may be some differences in the magnitudes and distribution of pinning centers. However, it is possible that multiple mechanisms can affect the onset of the Rayleigh regime, and the percentage of E_c that corresponds to the onset of the Rayleigh regime may differ with temperature.

These results were combined with Rayleigh analysis to understand the differences in the contributions to the dielectric response. Rayleigh analysis was performed as a function of temperature from 10 K up to 296 K for PZT films on Ni and Si substrates, as shown in Fig. 4. The Rayleigh coefficients were determined using a linear fit of the permittivity data vs electric field. The linear fits were taken for a minimum of five points above the corresponding E_{δ_3} for that temperature and sample. The Rayleigh coefficients of $\varepsilon_{\text{init}}$ [Fig. 4(c)] and α_{ray} [Fig. 4(d)] are plotted as a function of temperature for PZT on Ni (red squares) and Si (green circles). As thermal energy was added to the films, $\varepsilon_{\text{init}}$ increased for both sample sets. However, changes in these coefficients with temperature occurred at slightly different rates for PZT on Si and Ni. PZT on Ni had ε_{init} of 188 ± 0.3

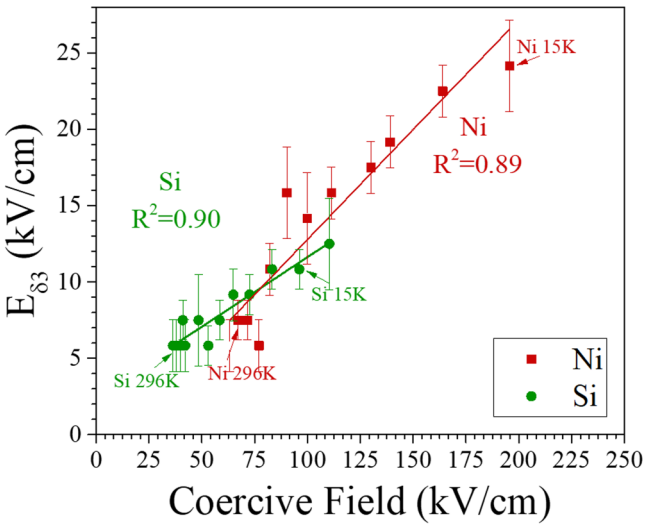

FIG. 3. E_{δ_3} vs coercive field for PZT on Ni (red square) and Si (green circle). From the slope (m) of these lines, it is estimated the Rayleigh regime begins around 9–14% of the coercive field for both PZT on Si and PZT on Ni.

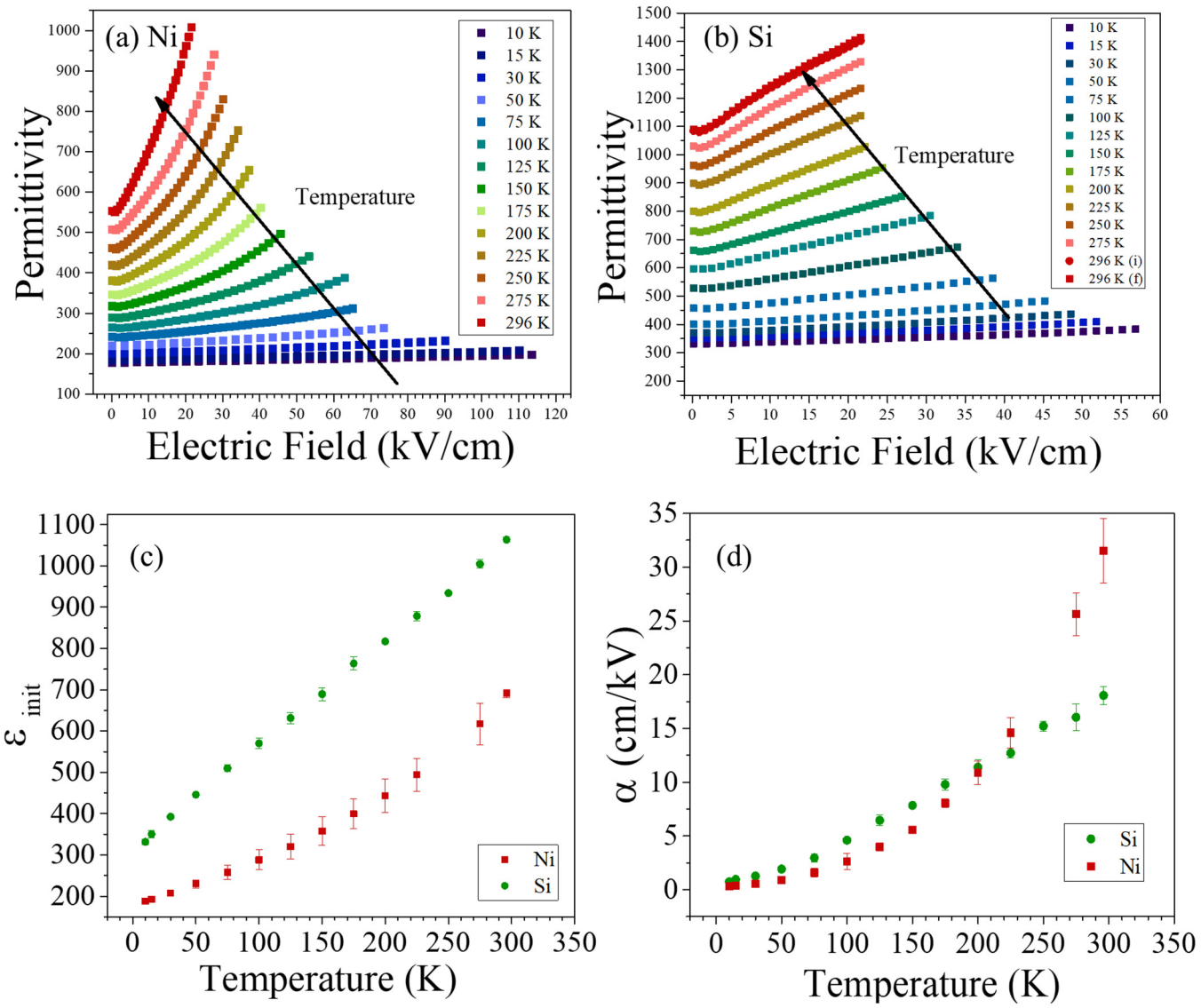

FIG. 4. Permittivity as a function of the electric field within the Rayleigh regime for (a) Ni and (b) Si samples. Rayleigh parameters of $\varepsilon_{\text{init}}$ (c) and α_{ray} (d) were plotted as a function of temperature for PZT films on both Ni (red squares) and Si substrates (green circles). Note: 296 K (i) indicates the permittivity values at room temperature at the start of the experiment and 296 K (f) indicates the values at room temperature after the experiment. The lack of clear differences indicates that the sample had minimal aging through the experiment.

at 10 K and 690 ± 8 at 296 K, and PZT on Si had a ε_{init} of 326 ± 0.3 at 10 K and 1065 ± 3 at 296 K.

At room temperature, α_{ray} is larger for PZT on Ni than Si, which may be due to the flexibility of the Ni foil. The Ni foil substrate produces less clamped films compared to PZT on Si, leading to more mobile domain walls.[28] As the temperature decreases, α_{ray} converges to zero near 10 K. The rate at which α_{ray} decreases is different for PZT on Ni and PZT on Si, suggesting that irreversible domain wall motion "freezes out" differently for these two types of samples. At 10 K, α_{ray} is 0.33 ± 0.01 cm/kV for PZT on Ni and 0.56 ± 0.03 cm/kV for PZT on Si. For temperature below 200 K, α_{ray} is higher for PZT films on Si relative to Ni, but this order reverses near room temperature.

To investigate the differences in the irreversible contribution, the $\alpha_{\text{Ray}}/\varepsilon_{\text{init}}$ ratio was determined for the two samples in Fig. 5. These differences in α_{ray} and $\alpha_{\text{Ray}}/\varepsilon_{\text{init}}$ as a function of temperature could be due to either differences in the domain structure or differences in the energy barrier height distribution. It is estimated that

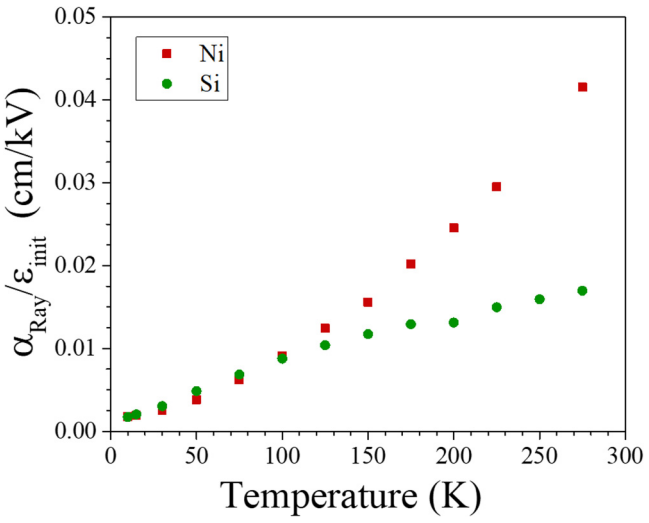

FIG. 5. $\alpha_{Ray}/\varepsilon_{init}$ ratio for PZT on Ni (red squares) and on Si (green circles).

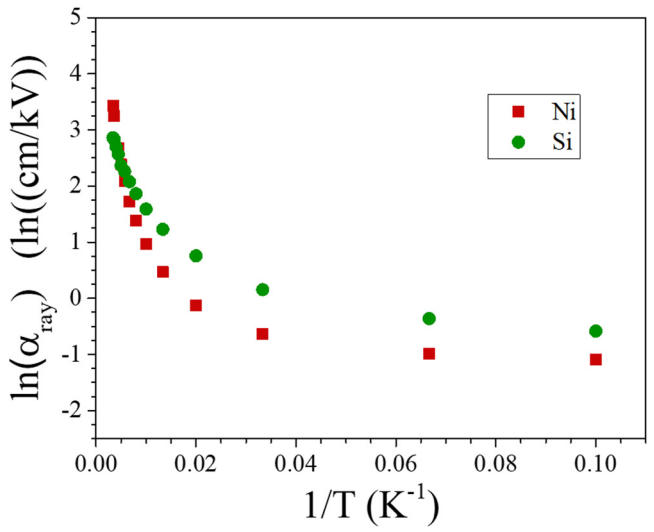

FIG. 6. Arrhenius plot of the natural log of α_{ray} vs 1/T to determine the ranges of activation energies for irreversible domain wall motion for PZT on Ni (red circle) and PZT on Si (green square). From the slope, the calculated activation energy at higher temperatures (from a linear fit form 225 K to 296 K) PZT on Ni and Si was 32.4 ± 3.2 meV and 16.9 ± 1.1 meV, respectively.

PZT on Si has roughly 40–60% "c" domains, and PZT on Ni has a higher percentage of "c" domains (around 80–95%).[23,49,63] Thus, it is likely that PZT films on Si have more non-180° domain walls. Since any motion of non-180° domain walls produces a large change in permittivity (as "a" and "c" domains have very different permittivity values), this could account for the higher α_{ray} at lower temperatures. However, this theory would be inconsistent with reports of limited amount of ferroelastic domain wall motion in films.[24,27] Therefore, it is more likely that there are lower energy barrier heights for PZT on Si, allowing for a slightly greater α_{ray} at lower temperatures. This is also supported by the increase in the magnitude of stress on the PZT film on Ni [calculated by Eq. (4)]. This may cause increase in pinning centers energies of the PZT on Ni and lead to the larger decay of α_{ray} with temperature.

Rayleigh behavior is observed when there is a Gaussian distribution of the restoring forces for domain walls. Presumably, as the temperature decreases, a smaller fraction of the distribution can be sampled for a given electric field. As a semi-quantitative approach to describing this, an Arrhenius-type plot was made for α_{ray} to approximate some average value for a pseudo-activation energy for domain wall motion at each temperature (see Fig. 6). Above 250 K, the pseudo-activation energies for PZT films on Ni and Si are 32.4 ± 3.2 meV and 16.9 ± 1.1 meV, respectively. At room temperature, there is ~25 meV available, suggesting that without the presence of electric fields some domain walls are mobile. This observation is consistent with the common observation of aging of properties that depend on domain wall motion. Comparing the two activation energies, PZT on Ni has higher pseudo-activation energies, which is consistent with the larger E_c and $E_{\delta 3}$. As the temperature decreased, the pseudo-activation energies also decreased. That is, when the thermal energy is low, irreversible domain wall motion from deeper wells may be frozen out in these systems; since only the shallower wells can be sampled, the pseudo-activation energies drop with decreasing temperature. As the temperature increases, deeper wells can be overcome with the increase in thermal energy; a rise in activation energies and α_{ray} value follows. This occurs at a steeper rate for PZT films on Ni.

The Rayleigh behavior and the phase angles of the dielectric constant indicate significant differences in the domain wall motion at modest electrical fields. To investigate higher fields, FORC loops were measured for PZT films on Ni (Fig. 7) and on Si (Fig. 8) substrates, from 15 K to 296 K. At lower temperatures, the FORC loops are squarer. As the temperature increased for both films, the polarization of the loops decreased and becomes tilted. PZT films on Si had lower P_r, which is consistent with the hysteresis loops in Fig. 1. This is believed to be differences in the residual stresses and the percentage of in-plane and out-of-plane domains in the two films.[20] The films on Ni are consistently under compressive stresses and, therefore, will have more out-of-plane domains and the higher P_r for all temperatures measured.

The reversible (P_{rev}) and irreversible (P_{irr}) FORC distributions were determined. Figure 9 shows the reversible Preisach distribution. P_{rev} is the part of the hysteron distribution that corresponds to the up (E_f) and down (E_b) switching fields being equivalent. P_{rev} for PZT on Si was symmetrical around 0 kV/cm; however, this was not the case for PZT on Ni for all electrodes measured. As the temperature increased, the peak magnitude increased for both PZT on Ni and Si. The reversible peak was much larger for PZT on Si than PZT on Ni. The typical shape of the hysteresis loops confirms this (Figs. 1, 7, and 8), as PZT on Si has a tilted hysteresis loop compared to PZT on Ni. The differences in the shape of the loop would suggest some differences in the Preisach distributions for the two films.

The P_{irr} distribution (where $E_f \neq E_b$) is shown in Figs. 10 and 11 for PZT on Ni and Si, respectively. PZT on Ni had a clear peak

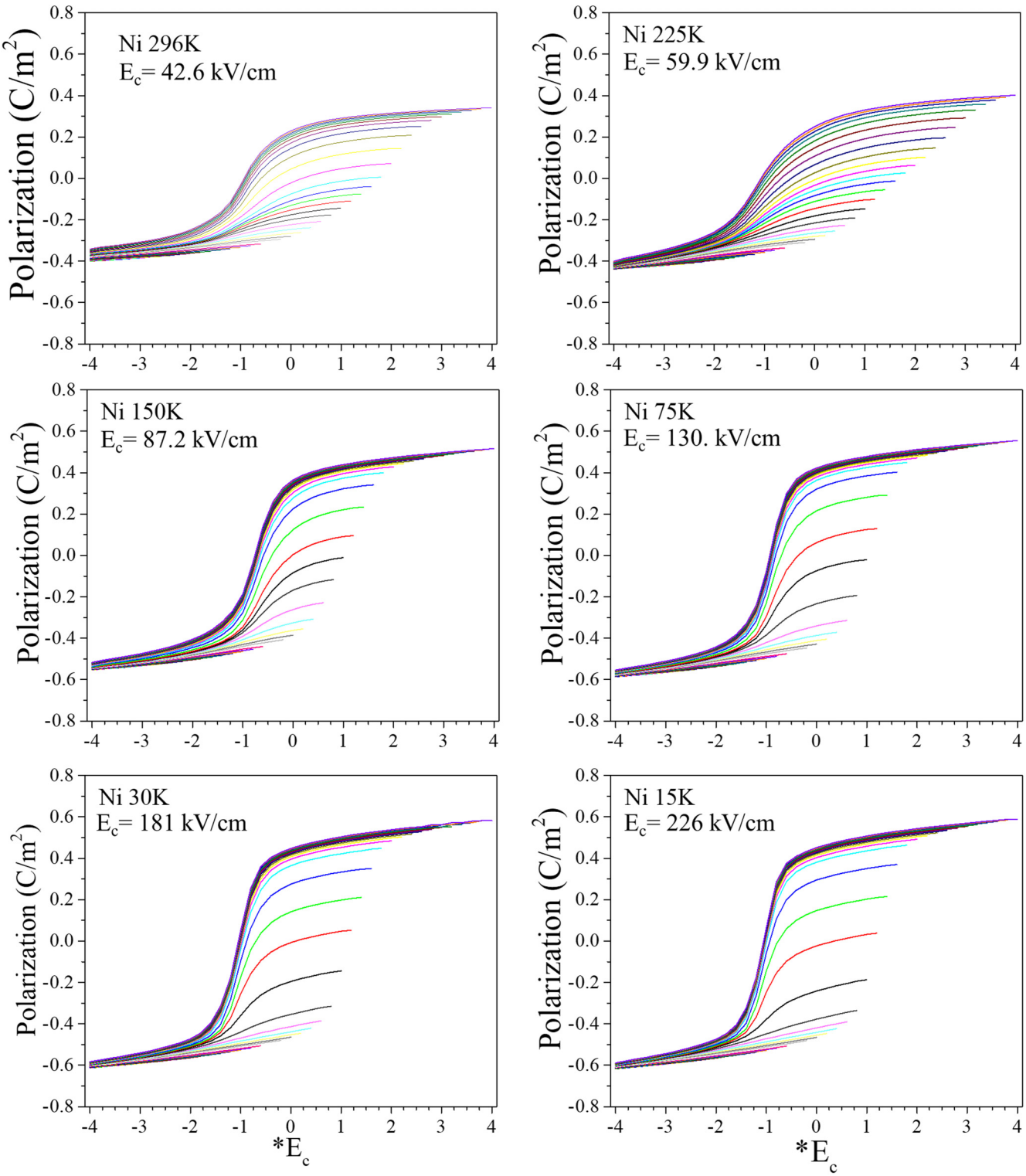

FIG. 7. FORC Loops for PZT films on Ni at 296 K, 225 K, 150 K, 75 K, and 15 K. The field range was from $-4E_c$ to $+4E_c$ for each temperature.

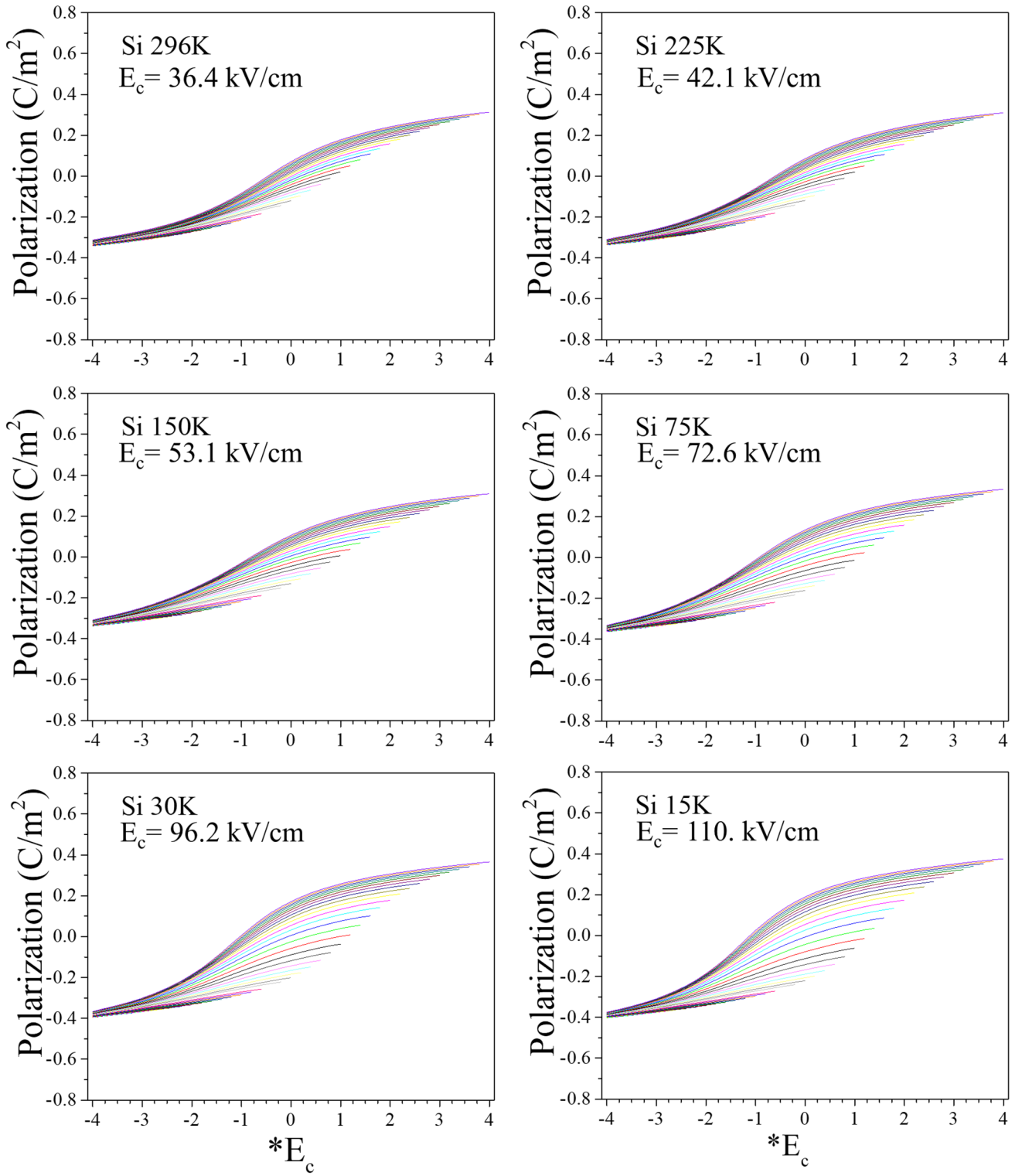

FIG. 8. FORC loops for PZT films on Si at 296 K, 225 K, 150 K, 75 K, and 15 K. The field range was from $-4E_c$ to $+4E_c$ for each temperature.

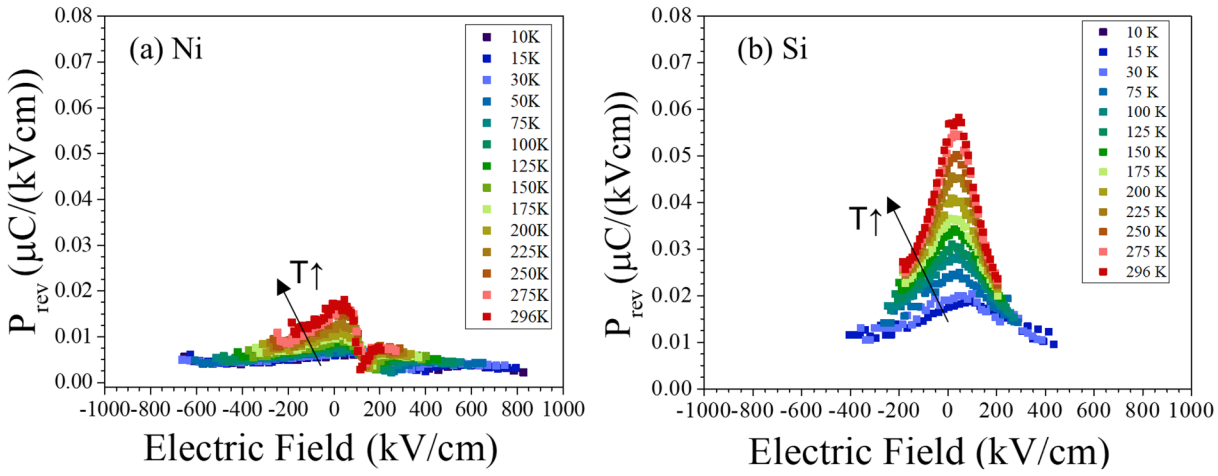

FIG. 9. Reversible FORC data, P_{rev} for PZT films on Ni (a) and PZT films on Si (b). P_{rev} for PZT on Si was 2–3 times larger than PZT on Ni.

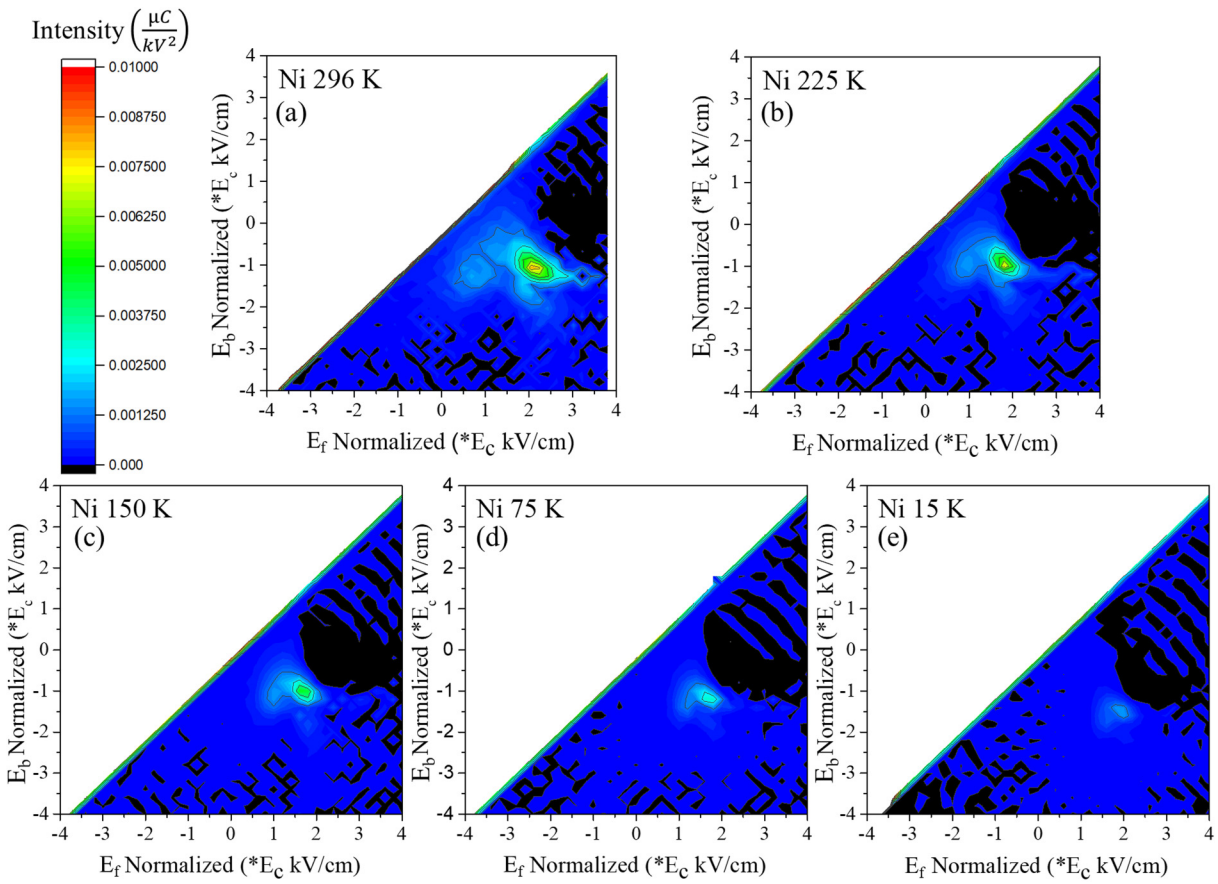

FIG. 10. P_{irrev} for PZT on Ni at 296 K (a), 225 K (b), 150 K (c), 75 K (d), and 15 K (e). E_f and E_b are normalized to four times E_c at the reported temperature.

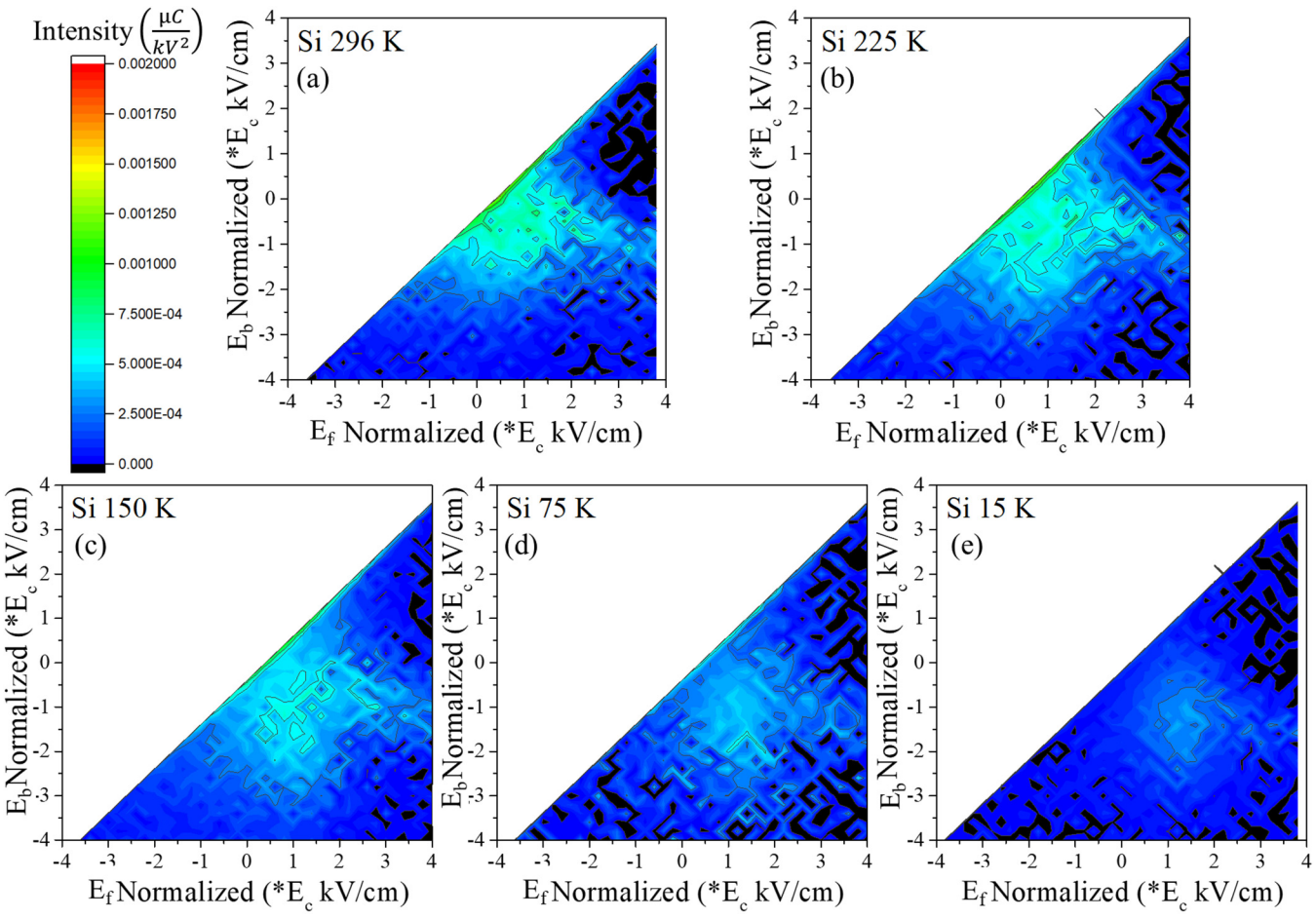

FIG. 11. P_{irrev} for PZT on Si at 296 K (a), 225 K (b), 150 K (c), 75 K (d), and 15 K (e). E_f and E_b are normalized to $4E_c$ at the reported temperature.

around $E_f = 2 \times E_c$, $E_b = -E_c$ for each respective temperature. The location of this peak may be due to imprint in the sample from poling prior to the FORC loop. As the temperature increased, this peak broadens and the intensity increased. This suggests that as the temperature increases, more hysterons can switch. This is consistent with the increase in the P_{rev} distribution. It is not clear how an individual pinning center's barrier heights change with temperature. However, the decrease in residual stress at higher temperatures for PZT on Ni may change individual barrier heights.

PZT on Si (Fig. 11) does not show a clear peak but does show a wide distribution of hysterons (note the scale difference between Figs. 10 and 11). This may suggest differences in the distribution of barrier heights between PZT on Ni and on Si. The center of P_{irr} on Si gradually moves closer to the $E_f = E_b$ line as the temperature increases, producing a more reversible response and a more tilted hysteresis loop.

These electrical characterization techniques show some variations in the distributions and barrier heights for domain wall motion and domain reorientation in films on Ni and Si. Figure 12 illustrates the differences in this barrier distribution schematically. PZT on Ni and Si exhibit Rayleigh behavior and Gaussian-like pinning center distribution. However, as indicated by the δ_3, this distribution does not continue to 0 eV, but down to 10–15% of E_c. It is unlikely that the tail of the Gaussian distribution reaches 0 as shown in Fig. 12.

PZT on Si has lower pseudo-activation energies, E_c and $E_{\delta 3}$ at each temperature. If it is assumed the same number of hysterons in each sample, then the PZT on Si would be expected to have more hysterons with lower energies. As a result, the center of the distribution is shifted to the left for PZT on Si compared to PZT on Ni. As indicated by the larger pseudo-activation energies, coercive fields and larger irreversible Preisach density for PZT on Ni, the center of the barrier height distribution is expected to be at a higher energy than PZT on Si. The lower energy barrier heights for PZT on Si allows for a slightly greater α_{ray} at lower temperatures.

Because of the sharp Preisach peak and the large increase in α_{Ray} with temperature, it is anticipated that the PZT on Ni has a

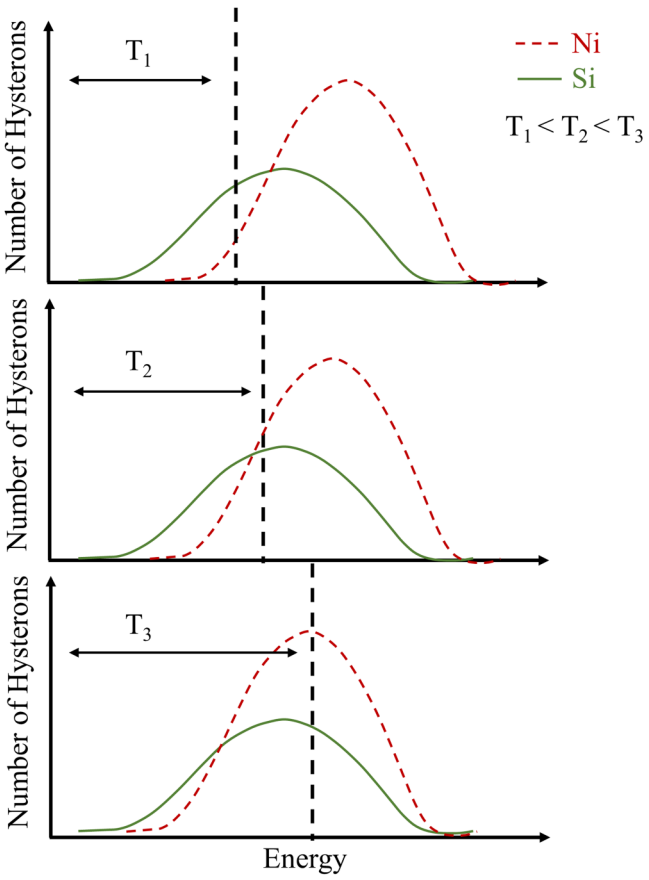

FIG. 12. Schematic of distribution of the population of hysterons with certain pinning energies for PZT on Ni (dashed red line) and Si (solid green curve). The horizontal dash black line represents the available energy at a given temperature. Any pinning center with lower energy levels is anticipated to be overcome at that temperature.

narrow distribution. Small increases in thermal energy will increase the number of switchable hysterons, noted by the increase in the area under the curve with higher temperatures (Fig. 12). Higher temperatures, in turn, increase the total energy in the system, allowing for more barriers to be overcome at the same exciting electric field. In the schematic Fig. 12, this increase would be represented by the area under the curved up to the dashed line, where the dashed line represents the energy available at each temperature. As the temperature increases, the dashed line would move further to the right, and more barriers could be overcome with the available energy. For the same temperature change (right shift of the dashed line) and the same number of total hysterons, the sample with the narrow distribution would see larger changes in the total number of hysterons that can be switched and in more domain wall motion. This is consistent for experimental observation of PZT on Ni. Assuming the same number of hysterons, the intensity of the Gaussian peak would be then larger for PZT on Ni.

Additionally, there is a temperature-induced stress change for PZT films on Ni. With decreasing temperature, the magnitude of the residual stress in the PZT layer increases. This increase in stress in the film may increase the depth of the potential wells for domain wall motion and lead to the rapid decrease in α_{ray} with decreasing temperature. Exactly how each individual pinning center changes with stress is unknown. To schematically represent this, the Ni pinning distribution could shift to the right with increasing temperature and reduction in the thermal expansion stress. This shift in the pinning distribution, the narrower distribution, or a combination of both would cause α_{ray} to increase more rapidly for PZT on Ni.

With various differences in extrinsic contributions of these films in mind, the pyroelectric coefficients at room temperature were further probed. Recalling Eq. (1), and the large differences in π, the different terms were explored. The secondary contribution, which combines stress and piezoelectric contributions, manifests in clamped thin films as Eq. (5) from the work of Zook *et al.*,[15]

$$\pi_{secondary} = \frac{2d_{31}(\alpha_f - \alpha_s)}{s_{11} + s_{12}}. \quad (5)$$

For PZT on Ni, $\pi_{secondary}$ was calculated to be approximately $-147\,\mu C/m^2\,K$, and for PZT on Si, $\pi_{secondary}$ is $45\,\mu C/m^2\,K$. The observed pyroelectric coefficient is the sum of the primary, extrinsic, and secondary term. Therefore, the primary plus extrinsic piece for PZT on Ni would be around $-100\,\mu C/m^2\,K$ and for PZT on Si would be around $-150\,\mu C/m^2\,K$. As shown by the larger P_r, PZT on Ni has more out-of-plane "c" domains and a larger primary piece. Therefore, for this sum to be smaller, the film on Ni must have a significantly smaller extrinsic piece. This smaller extrinsic term may be due to a different density of domain walls or higher pinning energies, which is suggested by the various electrical characterization techniques used in this study and schematically shown in Fig. 12.

Overall, this study suggests that the distribution of pinning centers for PZT films on Ni and Si are different; this induces different reversible and irreversible Rayleigh and Preisach distributions as a function of temperature. Given that the grain sizes are very similar for these two sets of films, it is believed that the residual stress accounts for at least some of the differences in the two families of films. Large differences in residual stresses will affect the film's domain structure, including the percentage of in-plane and out-of-plane domains and the energy landscape of various pinning sites for domain wall motion and domain switching. While these extrinsic contributions are typically considered to account for a small percentage of the total pyroelectric response, the combined influence of fabrication, stress, temperature on the domain structure, and substrate mechanical properties can result in a much more significant impact than one would expect.

CONCLUSIONS

PZT on Ni has a larger pyroelectric coefficient compared to PZT grown on Si, which is due to a large secondary contribution. However, the extrinsic contribution may be significantly reduced due to the residual stresses. PZT on Si and Ni have very different

reversible and irreversible Rayleigh and Preisach coefficients. It is proposed that larger differences in residual stresses drastically change the film's domain structure. Stress may allow for differences in the energy landscape of various pinning sites for domain wall motion and domain switching. These differences will lead to significant changes in the film's properties at various temperatures. With different energy barriers distributions, these films may have different optimal poling and driving conditions for high device performance. Further study should include defect chemistry, composition, and thickness on the distributions of pinning sites, as well as designing films/substrate stacks with lower energy barrier for domain wall motion to further improve the pyroelectric coefficient.

SUPPLEMENTARY MATERIAL

See the supplementary material for the higher harmonics of the dielectric displacement, permittivity and phase angle plots, estimates of percentage of "c" domains from phenomenology, and determination of the Curie temperature for films on Ni and Si.

ACKNOWLEDGMENTS

This material is based upon work supported by the National Science Foundation as part of the Center for Dielectrics and Piezoelectrics under Grant Nos. IIP-1361571, IIP-1361503, IIP-1841453, and IIP-1841466.

The authors would like to acknowledge Jeff Long at the Materials Research Institute and Penn State University for the help with the experimental setup.

DATA AVAILABILITY

The data that support the findings of this study are available from the corresponding author upon reasonable request.

REFERENCES

[1]R. W. Whatmore, Rep. Prog. Phys. **49**, 1335 (1986).
[2]N. M. Shorrocks, A. Patel, M. J. Walker, and A. D. Parson, Microelectron. Eng. **29**, 59 (1995).
[3]D. Setiadi, H. Weller, and T. D. Binnie, Sens. Actuators A **76**, 145 (1999).
[4]R. W. Whatmore, Q. Zhang, C. P. Shaw, R. A. Dorey, and J. R. Alcock, Phys. Scr. **T129**, 6 (2007).
[5]R. B. Olsen, D. A. Bruno, and J. M. Briscoe, J. Appl. Phys. **58**, 4709 (1985).
[6]Z. Zhang, B. Hanrahan, C. Shi, and A. Khaligh, Appl. Energy **230**, 1326 (2018).
[7]S. Pandya, G. A. Velarde, R. Gao, A. S. Everhardt, J. D. Wilbur, R. Xu, J. T. Maher, J. C. Agar, C. Dames, and L. W. Martin, Adv. Mater. **31**, 1803312 (2019).
[8]J. Cooper, J. Sci. Instrum. **39**, 467 (1962).
[9]R. Bruchhaus, D. Pitzer, R. Primig, M. Schreiter, and W. Wersing, Integr. Ferroelectr. **25**, 1 (1999).
[10]R. W. Whatmore, J. Electroceram. **13**, 139 (2004).
[11]P. Muralt, Rep. Prog. Phys. **64**, 1339 (2001).
[12]M. E. Lines and A. M. Glass, *Principles and Applications of Ferroelectrics and Related Materials* (Oxford University Press, 1977).
[13]G. Velarde, S. Pandya, L. Zhang, D. Garcia, E. Lupi, R. Gao, J. D. Wilbur, C. Dames, and L. W. Martin, ACS Appl. Mater. Interfaces **11**, 35146 (2019).
[14]I. Lubomirsky and O. Stafsudd, Rev. Sci. Instrum. **83**, 051101 (2012).
[15]J. D. Zook and S. T. Liu, J. Appl. Phys. **49**, 4604 (1978).
[16]Y. Ivry, V. Lyahovitskaya, I. Zon, I. Lubomirsky, E. Wachtel, and A. L. Roytburd, Appl. Phys. Lett. **90**, 172905 (2007).
[17]J. Karthik, J. C. Agar, A. R. Damodaran, and L. W. Martin, Phys. Rev. Lett. **109**, 257602 (2012).
[18]B. Hanrahan, Y. Espinal, C. Neville, R. Rudy, M. Rivas, A. Smith, M. T. Kesim, and S. P. Alpay, J. Appl. Phys. **123**, 124104 (2018).
[19]S. Pandya, G. A. Velarde, R. Gao, A. S. Everhardt, J. D. Wilbur, R. Xu, J. T. Maher, J. C. Agar, C. Dames, and L. W. Martin, J. Adv. Mater. **37**, 1803312 (2019).
[20]B. A. Tuttle, J. A. Voigt, T. J. Garino, D. C. Goodnow, R. W. Schwartz, D. L. Lamppa, T. J. Headley, and M. O. Eatough, in *ISAF '92 Proceedings of the Eighth IEEE International Symposium on Applications of Ferroelectrics* (IEEE, Greenville, SC, 1992), Vol. 344.
[21]M. D. Nguyen, M. Dekkers, E. Houwman, R. Steenwelle, X. Wan, A. Roelofs, T. Schmitz-Kempen, and G. Rijnders, Appl. Phys. Lett. **99**, 252904 (2011).
[22]J. J. Wang, Y. Wang, J. F. Ihlefeld, P. E. Hopkins, and L. Q. Chen, Acta Mater. **111**, 220 (2016).
[23]K. Coleman, J. Walker, T. Beechem, and S. Trolier-McKinstry, J. Appl. Phys. **126**, 034101 (2019).
[24]R. J. Zednik, A. Varatharajan, M. Oliver, N. Valanoor, and P. C. McIntyre, Adv. Funct. Mater. **21**, 3104 (2011).
[25]H. G. Yeo and S. Trolier-McKinstry, J. Appl. Phys. **116**, 014105 (2014).
[26]H. Hoshyarmanesh, N. Nehzat, M. Salehi, and M. Ghodsi, J. Mech. Sci. Technol. **29**, 715 (2015).
[27]M. Wallace, R. L. Johnson-Wilke, G. Esteves, C. M. Fancher, R. H. T. Wilke, J. L. Jones, and S. Trolier-McKinstry, J. Appl. Phys. **117**, 054103 (2015).
[28]L. M. Denis, G. Esteves, J. Walker, J. L. Jones, and S. Trolier-McKinstry, Acta Mater. **151**, 243 (2018).
[29]D. Damjanovic and M. Demartin, J. Phys. D. Appl. Phys. **29**, 2057 (1996).
[30]N. Bassiri-Gharb, I. Fujii, E. Hong, S. Trolier-McKinstry, D. V. Taylor, and D. Damjanovic, J. Electroceram. **19**, 49 (2007).
[31]K. Kuramoto and E. Nakamura, Ferroelectrics **157**, 57 (1994).
[32]D. V. Taylor and D. Damjanovic, Appl. Phys. Lett. **73**, 2045 (1998).
[33]R. E. Eitel, T. R. Shrout, and C. A. Randall, J. Appl. Phys. **99**, 124110 (2006).
[34]S. Shetty, *Electromechanical Characterization of Lead Magnesium Niobate Based Thin Films*, Ph.D (Pennsylvania State University, 2019).
[35]F. Preisach, Z. Phys. **94**, 277 (1935).
[36]G. Robert, D. Damjanovic, N. Setter, and A. V. Turik, J. Appl. Phys. **89**, 5067 (2001).
[37]A. T. Bartic, D. J. Wouters, H. E. Maes, J. T. Rickes, and R. M. Waser, J. Appl. Phys. **89**, 3420 (2001).
[38]W. Zhu, I. Fujii, W. Ren, and S. Trolier-McKinstry, J. Appl. Phys. **109**, 064105 (2011).
[39]B. Akkopru-Akgun, W. Zhu, M. T. Lanagan, and S. Trolier-McKinstry, J. Am. Ceram. Soc. **102**, 5328 (2019).
[40]F. Wolf, A. Sutor, S. J. Rupitsch, and R. Lerch, Sens. Actuators A. **186**, 223 (2012).
[41]R. K. Vasudevan, D. Marincel, S. Jesse, Y. Kim, A. Kumar, S. V. Kalinin, and S. Trolier-McKinstry, Adv. Funct. Mater. **23**, 2490 (2013).
[42]D. Piazza, L. Stoleriu, L. Mitoseriu, A. Stancu, and C. Galassi, J. Eur. Ceram. Soc. **26**, 2959 (2006).
[43]P. Muralt, R. G. Polcawich, and S. Trolier-McKinstry, MRS Bull. **34**, 658 (2009).
[44]N. Izyumskaya, Y. I. Alivov, S. J. Cho, H. Morkoç, H. Lee, and Y. S. Kang, Crit. Rev. Solid State Mater. Sci. **32**, 111 (2007).
[45]D. Dimos, R. W. Schwartz, and S. J. Lockwood, J. Am. Ceram. Soc. **77**, 3000 (1994).
[46]T. Tani and D. A. Payne, J. Am. Ceram. Soc. **77**, 1242 (1994).
[47]I. Fujii, E. Hong, and S. Trolier-McKinstry, IEEE Trans. Ultrason. Ferroelectr. Freq. Control **57**, 1717 (2010).
[48]L. Jin, V. Porokhonskyy, and D. Damjanovic, Appl. Phys. Lett. **96**, 242902 (2010).
[49]M. J. Haun, E. Furman, S. J. Jang, and L. E. Cross, Ferrolectrics **99**, 63 (1989).

[50]C. B. Yeager, Y. Ehara, N. Oshima, H. Funakubo, and S. Trolier-McKinstry, J. Appl. Phys. **116**, 104907 (2014).
[51]M. Murakami, J. Vac. Sci. Technol. A **9**, 2469 (1991).
[52]A. T. Nettles, "Basic Mechanics of Laminated Composites Plates," NASA Report No. NA-RP-351, 1994.
[53]L. Jordan and W. H. Swanger, Bur. Stand. J. Res. **5**, 1291 (1930).
[54]Y. S. Touloukian, R. K. Kirby, R. E. Taylor, and P. D. Desal, "Thermophysical properties of matter—The TPRC data series," in *Thermal Expansion Metallic Elements and Alloys* (Purdue University, 1975), Vol. 12.
[55]Y. Okada and Y. Tokumaru, J. Appl. Phys. **56**, 314 (1984).
[56]Y. S. Touloukian, R. K. Kirby, R. E. Taylor, and T. Y. R. Lee, "Thermophysical properties of matter-The TPRC data series," in *Thermal Expansion Nonmetallic Solids* (Purdue University, 1975), Vol. 13.
[57]M. J. Haun, E. Furman, H. A. McKinstry, and L. E. Cross, Ferroelectrics **99**, 27 (1989).
[58]W. R. Cook, D. A. Berlincourt, and F. J. Scholz, J. Appl. Phys. **34**, 1392 (1963).
[59]B. Noheda, D. E. Cox, G. Shirane, J. A. Gonzalo, L. E. Cross, and S. E. Park, Appl. Phys. Lett. **74**, 2059 (1999).
[60]D. E. Cox, B. Noheda, G. Shirane, Y. Uesu, K. Fujishiro, and Y. Yamada, Appl. Phys. Lett. **79**, 400 (2001).
[61]A. J. Bell and E. Furman, in *IEEE International Symposium on Applications on Ferroelectrics* (IEEE, Nara, Japan, 2002), Vol. 19.
[62]M. I. Morozov and D. Damjanovic, J. Appl. Phys. **104**, 034107 (2008).
[63]M. J. Haun, Z. Q. Zhuang, E. Furman, S. J. Jang, and L. E. Cross, Ferroelectrics **99**, 45 (1989).